R - CURVE BEHAVIOUR OF Al-Li-Cu-Mg ALLOYS

N. ESWARA PRASAD*, M. RAMULU** AND G. MALAKONDAIAH*

* Defence Metallurgical Research Laboratory, P.O. Kanchanbagh, Hyderabad - 500 058, India
** Dept. of Mechanical Engineering, University of Washington, Seattle, WA, 98195 - 2600, USA

ABSTRACT

K_R - Δa data have been obtained for Al-Li alloys AA 8090 (in underaged, T3 and peakaged, T6 tempers) as well as AA 2090 (in peakaged, T6 temper) in L - T and T - L test orientations. The nature of R-curves was found to be a function of composition, temper condition and also, the notch orientation. The micro-mechanisms of fracture process have been studied using replica technique. The observed R - curve behaviour has been rationalised with the help of the prevailing fracture mechanisms and the nature of microstructure - crack path interactions.

KEYWORDS

Plane stress fracture resistance, Al - Li alloys, microstructure, crack paths, fracture mechanism.

INTRODUCTION

Aluminium - lithium alloys have received considerable research interest in recent years because of their potential for aerostructural applications owing to their superior specific strength and stiffness (Grimes et al., 1985). However, significant improvements in tensile ductility and fracture toughness are required in order for these alloys to replace the traditionally used 2XXX and 7XXX aluminium alloys (Starke and Lin, 1982; Wanhill, 1994). Studies on fracture resistance have mainly dealt with plate products and thereby essentially been limited to plane - strain loading conditions (Gregson and Flower, 1985; Jata and Starke, 1986; Suresh et al., 1987; Lynch, 1991). Similar studies on sheet products, where plane-stress loading conditions prevail, have been limited (McDarmaid and Peel, 1989; Peel and McDarmaid, 1989; Kamat and Eswara Prasad, 1990; Wanhill et al., 1992; Eswara Prasad et al., 1993, 1995). In the present paper, we present the plane - stress fracture resistance (R - curve) behaviour of Al-Li alloy sheets of varied composition as well as heat treatment condition and also, the notch orientation. The prevailing fracture mechanisms and the fracture process are also described.

EXPERIMENTAL METHODS

The chemical composition of the alloys is presented in Table 1. The AA2090 alloy is a ternary alloy with higher copper and marginally lower lithium as compared to the quaternary alloy AA8090. Both the alloys exhibit pancake microstructure with varied degree of recrystallisation. The microstructural details of the alloys, described in detail elsewhere (Eswara Prasad et al., 1995), are summarised in Table 2. Plane - stress fracture toughness tests were conducted on the alloy sheets in L-T (notch being oriented perpendicular to the rolling direction) and T-L (notch being oriented parallel to the rolling direction) orientations. Compact tension specimens of width 101.6mm and half-width to height ratio of 0.6 were employed to determine the fracture toughness. The thickness of the specimens was that of the parent sheet material (see Table 2). The specimens were precracked under fatigue loading at a stress intensity factor range of 8-12 MPa $\sqrt{m}$ with an R-ratio of 0.1. Precracked specimens were pulled in tension at a constant ramp rate of 0.5mm/min.. The tests were conducted on a computer controlled servohydraulic MTS 880 test system. Crack extension (Δa) was monitored using unloading compliance technique with the help of a 5mm crack opening displacement (COD) gauge. The computed crack length measurements were verified optically with the help of a travelling microscope. The fracture resistance (K_R) of the alloys was evaluated as per ASTM standard E - 561 (1990).

Specimens of 1T CT in-plane dimensions, but with the specimen thickness the same as the sheet thickness, were used to register the crack path - microstructure interactions as well as the crack growth mechanisms. The specimens in metallographically polished condition were pulled in tension as per the procedure described above and were held at each step corresponding to a crack extension of ~ 0.2mm. Replicas obtained at these interruptions were examined using optical and stereo-optical microscopes as well as scanning electron microscope (SEM). For SEM observations, the replicas were coated with Au-Pd alloy. Polished specimens in etched condition were also examined at different stages of crack extension in order to register crack path - microstructure interactions.

Table 1. Nominal Composition of the Al - Li Alloys

Alloy Designation	Alloying Elements, wt.%						
	Li	Cu	Mg	Zr	Fe	Si	Al
AA8090	2.2	1.05	0.73	0.12	0.046	0.02	Bal.
AA2090	2.1	2.97	0.04	0.10	0.09	< 0.01	Bal

RESULTS AND DISCUSSION

R - Curves and Crack Path Morphologies

Al - Li alloy AA8090

K_R - Δa data obtained in the L-T and T-L orientations of the Al - Li alloy AA8090 in peakaged (T6) condition are shown in Fig.1. The data show closely matching K_c values in both the test directions (Table 2). However, the growth resistance, as depicted by the rise in K_R with Δa, is found to be higher in L-T orientation as compared to that in T-L orientation. The crack path morphologies

Table 2. Microstructural Details and Plane - Stress Fracture Toughness Data of Al - Li Alloy Sheets

Description		AA8090 - T6 (3mm thick)	AA8090 - T3 (6mm thick)	AA2090 - T6 (4.5mm thick)
Microstructure :				
Microstructure		Pancake	Pancake	Pancake
Degree of recrystallisation (%)		20 - 25	80	20 - 30
Intragranular precipitates				
(a) Al_3Li (δ')		High density (10nm diameter)	High density (5nm diameter)	High density (10nm diameter)
(b) Al_2CuMg (S)		Low density	Low density	Low density
(c) Al_2CuLi (T_1)		Low density	Low density	High density
Intergranular precipitates				
(a) Al_6CuLi_3 (T_2)		High density	Present	Low density
(b) Coarse T_1		Present	Present	High density
(c) Al_2Cu (θ)		Not present	Not present	High density
Width of δ' - precipitate free zone (nm)		100	30 - 40	5 - 10
Mechanical Properties :				
0.2% yield strength (MPa)	L*	455	365	455
	LT*	435	360	460
Plane stress fracture toughness, K_c (MPa$\sqrt{m}$)	L - T	54	123	72
	T - L	48	91	46
Maximum fracture resistance $K_{max.}$ (MPa $\sqrt{m}$)	L - T	58	132**	87**
	T - L	52	101	50
Nature of R - curves	L - T	Moderately Rising	Rising	Rising
	T - L	Flat	Moderately Rising	Flat
Nature of crack paths	L - T	Deflected	Deflected	Deflected & branched
	T - L	Straight	Deflected	Straight

* L - longitudinal, axis parallel to the rolling direction; LT - long-transverse, axis perpendicul to the rolling direction.

** Maximum values of K_R obtained experimentally, as the corresponding K_R - Δa curves show no indication of saturation.

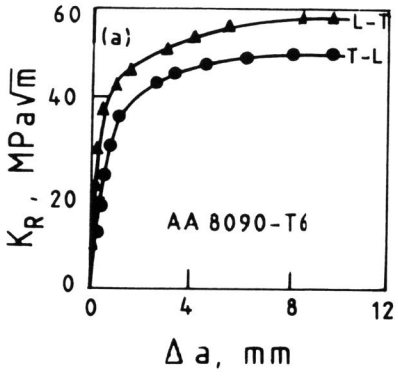

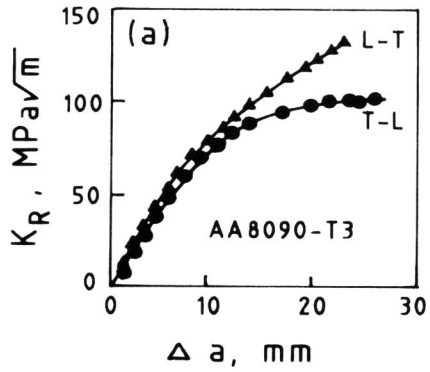

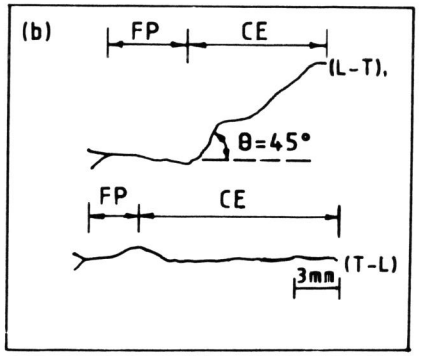

Fig.1. K_R - Δa curves (a) and the corresponding crack path morphologies (b) of the Al - Li alloy AA8090 - T6 in L - T and T - L orientations. (FP - Fatigue Precrack; CE - Crack Extension)

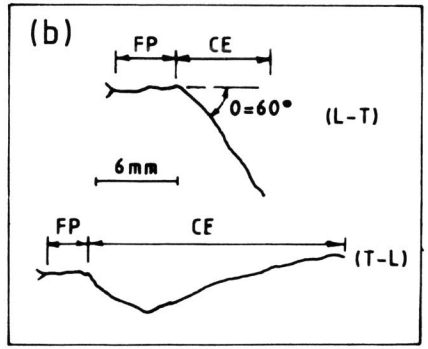

Fig.2. K_R - Δa curves (a) and the corresponding crack path morphologies (b) of the Al - Li alloy AA8090 - T3 in L - T and T - L orientations. (FP - Fatigue Precrack; CE - Crack Extension)

in the two test directions are included in Fig.1. These show a deflected crack with an average angle of deflection, θ = 45° (oriented in mixed mode I/II) in L-T orientation and a nominally straight (oriented in mode I) in T-L orientation. K_R - Δa data and corresponding crack path morphologies of Al - Li AA8090 alloy in the underaged (T3) condition are shown in Fig.2. The underaged AA8090 alloy exhibits moderately rising R-curve with crack path deflection even in T-L orientation. Further, the R-curve in L- T orientation for the underaged condition is steeply rising with no apparent saturation and the crack path is considerably deflected, with an average deflection angle of 60°.

Al - Li alloy AA2090

The R-curves and the corresponding crack path morphologies in L-T and T-L orientations of the alloy AA2090 - T6 are shown in Fig.3. The R-curve shows steeply rising behaviour in L-T orientation, while it remains nearly flat in T-L orientation. The crack path in L-T orientation is deflected (average angle of deflection, θ = 48°) with axi-asymmetrical branching (branch included angle, 2α = 45° and the ratio of branched crack ligament lengths, b/a of 2.2), while the same in T - L orientation is nominally straight. The difference in fracture resistance between L - T and T - L orientations was found to be more significant in this case as compared to the Al-Li alloy AA8090 in both underaged and peakaged conditions (Figs. 1 and 2; Table 2).

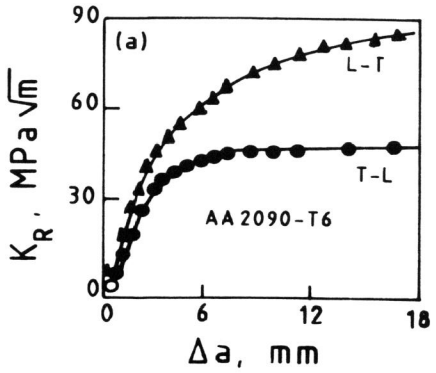

Fracture Process under Plane Stress Loading

In order to study the details of the fracture mechanisms, replicas of the surfaces of polished specimens, obtained at different values of K_R, were examined in a SEM. These studies revealed that the crack extension process in all the cases involves four distinct stages, namely (i) plastic zone formation, (ii) microcracking ahead of the main crack, (iii) coalescence of microcracks into a macrocrack, and finally (iv) linkage of the macrocrack with the main crack. These four stages for AA8090-T6 alloy are shown in Fig.4. The plastic zone formation (detectable during SEM observations) occurs as early as at 0.5 - 0.6K_c and plastic zone enlargement continues to happen till the advent of advanced microcracking. The advanced microcracking occurs at K_R values of 0.7-0.9 K_c and at this stage there occurs small load drops in the load - COD plots. This stage corresponds to K_R value corresponding to the point of deviation from linearity in K_R - Δa data occurs. With further increase in K_R, the advance microcracks coalesce to form macrocrack and the macrocrack merges with the initial main crack. There occurs a large load drop with the merger of macrocrack with the initial main crack. The first such event corresponds to K_R value corresponding to the point of deviation from linearity in K_R - Δa data. The load is subsequently recovered with the repetition of the four stages of crack growth. This process gets repeated leading to a stepwise crack extension.

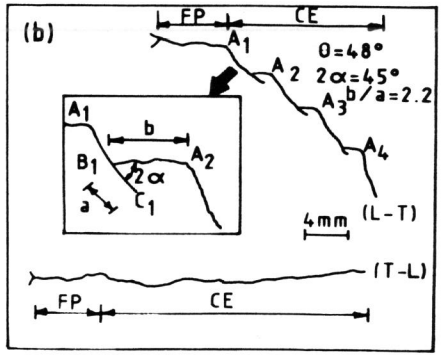

Fig.3. K_R - Δa curves (a) and the corresponding crack path morphologies (b) of the Al - Li alloy AA2090 - T6 in L - T and T - L orientations. (FP - Fatigue Precrack; CE - Crack Extension)

The interaction of crack path with various microstructural features leads to significant differences in the crack path morphology at a macrolevel for the two alloys. Crack path meandering (crack deflection and/or branching) occurs in L-T orientation, while it is nominally straight in T-L orientation. The surface appearances shown in Fig.5 represent various stages of crack initiation and growth for the alloy AA8090 - T6 in L-T and T-L orientations. Stage 1 of Fig.5 corresponds to crack initiation, while the rest of the macrographs represent the crack propagation. Initially, the crack extension takes place with branching. However, one of the branched crack ligaments only extends

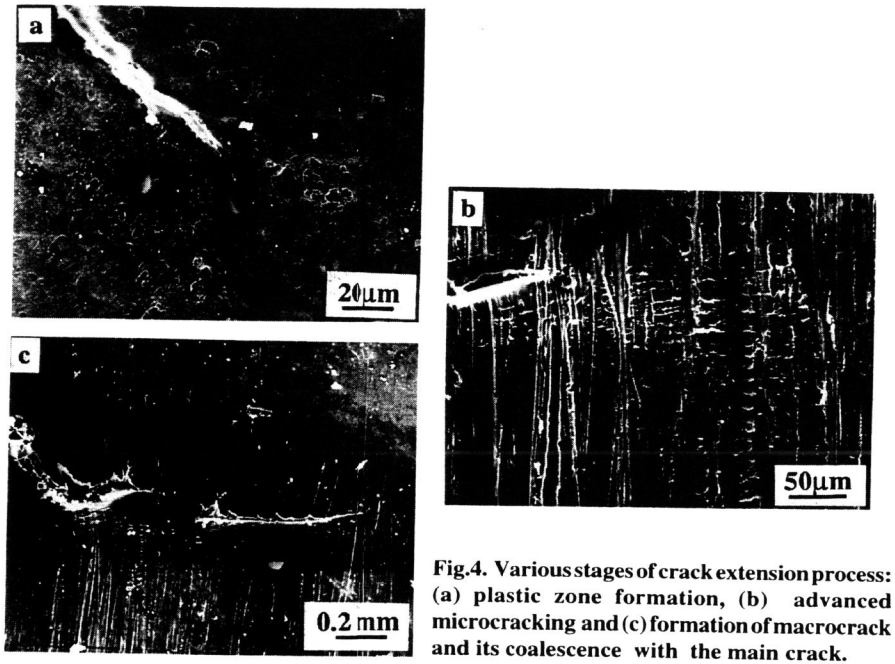

Fig.4. Various stages of crack extension process: (a) plastic zone formation, (b) advanced microcracking and (c) formation of macrocrack and its coalescence with the main crack.

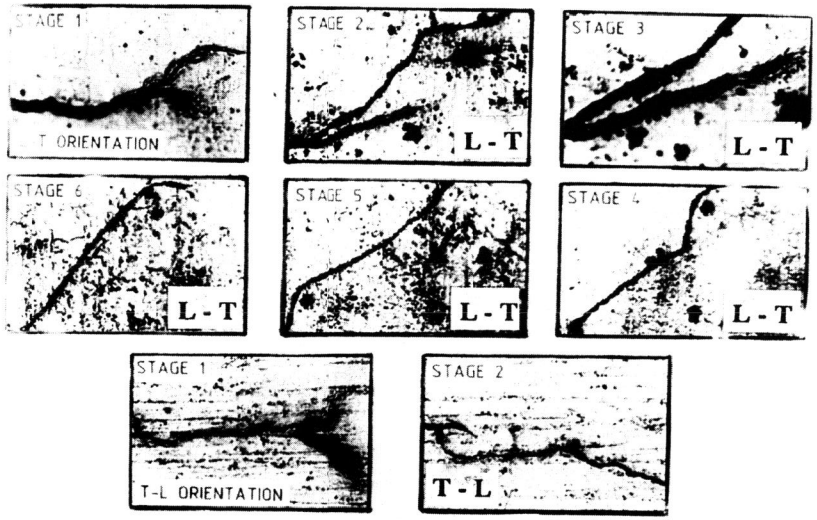

Fig.5. Various stages of main crack extension in AA8090-T6 alloy in L-T and T-L orientations

further preferentially leading to straight crack path in T-L orientation and deflected crack path in L-T orientation. The crack extension may takes place along high- or low- angle grain boundaries or along precipitate (in this case Al_3Li (δ') precipitates) slip bands, whichever is more favourable (Stark and Lin, 1982; Eswara Prasad et al., 1993). The presence of coarse intergranular precipitates, T_1 and /or T_2 (see Table 2), along high- angle grain boundaries promote crack extension along these boundaries. This results in straight crack extension in T-L orientation (stage 2 of T-L orientation in Fig.5). On the other hand, the crack extension along δ' - precipitate slip bands results in extension of one of the branched crack ligament which is orientated at an angle to the initial main crack. Further crack extension takes place along the inclined crack while the other ligamant gets arrested. The branch conditions, namely the values of the lengths of branched crack ligaments and the included angle, which depend on the local micromechanisms of crack extension and the associated effective stress intensity factor determine the nature of crack extension (Eswara Prasad et al., 1993). This finally results in a deflected crack at macro level (stages 2 - 6 of L-T orientation in Fig.5).

In the case of alloy AA2090 - T6, crack path deflection occurs with macrocrack branching (Fig.3b). This is because both the initially branched crack ligaments extend further as one of the ligaments is oriented along δ' - precipitate slip bands while the other along low - angle grain boundaries. The alloy AA2090, unlike alloy AA8090, has significant amount of coarse Al_2Cu (θ) precipitates along the low - angle grain boundaries. This promotes simultaneous crack extension along δ' - precipitate slip bands and the low - angle grain boundaries, resulting in asymmetrical branching.

Modelling of Crack Growth Resistance

R - curves of structural alloy sheets are normally steeply rising in nature with significant increase in K_R with crack extension. Such R - curves are the result of extensive crack tip plasticity and stable nature of crack growth. However, as described earlier, Al-Li alloys typically show flat R-curves in T -L orientation, with moderate to negligible increase in K_R and associated unstable crack extension (Wanhill, 1994; Eswara Prasad et al., 1995). On the other hand, AA2090 - T6 in L - T orientation, AA8090 - T3 alloy in L - T and T - L orientations and AA8090 - T6 in L - T orientation show typically rising R - curves (Figs.1 - 3). In these cases there is a significant increase in K_R with Δa, which can be seen once we note the difference between the values of plane - stress fracture toughness K_c and maximum fracture resistance $K_{max.}$ (see data in Table 2). This is due to the fact that these alloys in the aforementioned conditions show significant crack path deflection with or without crack branching. The increased K_R due to crack path deflection and branching can be predicted as (Kamat and Eswara Prasad, 1990; Eswara Prasad et al., 1993):

(a) for purely deflected crack : $$(K_R)_D = (K_R)_{UD} \, Sec^{1/2}\theta \quad (1)$$

(b) for purely branched crack : $$(K_R)_{Br} = (K_R)_{UBr} \{ \sum_{i=1}^{m} [F'(2\alpha, b/a) - 1]_m \} \quad (2)$$

(c) for deflected and branched crack :

$$(K_R)_{D,Br} = (K_R)_{UD,UBr} \, Sec^{1/2}\theta \{ 1 + \sum_{i=1}^{m} [F'(2\alpha, b/a) - 1]_m \} \quad (3)$$

where the subscripts UD, UBr and D, Br refer to undeflected, unbranched and deflected, branched cases, respectively. θ is the deflection angle and 2α , b/a are the branch characteristics i.e., branch included angle and ratio of the lengths of branched ligaments, respectively. F' is a numerical function

which depends upon the nature and characteristics of branching and m is the number of branch events. From equations (1) - (3), it can be inferred that at higher values of θ, F' and m, the rise in K_R will be higher. This physically means that if the extent of crack path deflection and branching is higher then so will be the rise in K_R. This would be the case if the crack extension occurs under mixed mode conditions. Several microstructural features were found to promote such crack path deflection and branching (Eswara Prasad et al., 1995). For example, for an asymmetically branched crack (see the nature of crack path of AA2090 - T6 alloy in L-T orientation shown in Fig.3b) of 2α equal to 45°, Eswara Prasad et al. (1993)have shown that the nature of crack extension depends upon the branch characteristics. For $b/a < 1.6$ the crack ligament 'a' extends further, while for $b/a > 1.8$ the crack ligament 'b' extends further. In actual situations the crack extension occurs through a complex process which combines the above modes and takes place with a constant variation in θ, 2α and b/a.

CONCLUSIONS

1. Al - Li alloys show significantly rising R - curves in L - T orientation and nearly flat R - curves in T - L orientation. The crack paths are highly meandered in the L - T orientation, while the same in T - L orientation are nominally straight.
2. Crack extension under monotonic loading goes through four distinct stages via. plastic zone formation, advanced microcracking, coalescence of microcracks to form a macrocrack and finally merger of macrocrack with the main crack.
3. The microstructural features strongly influence crack path morphology.

ACKNOWLEDGEMENTS

The authors thank Mr. S.L.N. Acharyulu, Director, DMRL for kind permission to publish these results. Thanks are due to Mr. S.Gupta for his help in conducting SEM work. The authors are grateful to Dr. P. Rama Rao, Distinguished Scientist, DRDO, for his constant encouragement and keen interest in this work.

REFERENCES

ASTM Standard E - 561 (1990), *American Society for Testing and Materials,* **Vol. 3 - 01**, 571 - 582.

Eswara Prasad, N., Kamat, S.V. and Malakondaiah, G., (1993), *Inter. J. Fract.*, **61**, 55 - 69.

Eswara Prasad, N., Prasad, K.S., Kamat, S.V. and Malakondaiah, G. (1995), *Eng. Fract. Mech.*, **51**, 87 - 96.

Gregson, P.J. and Flower, H.M. (1985), *Acta Metall.*, **35**, 527 - 537.

Grimes, R., Cornish, A.J., Miller, W.S. and Reynolds, M.A. (1985), *Metals Mater.*, **1**, 357 - 366.

Jata, K.V. and Starke, E.A. (1986), *Metall. Trans. A,* **17A**, 1011 - 1026.

Kamat, S.V. and Eswara Prasad, N. (1990), *Scripta Metall.*, **24**, 1907 - 1912.

Lynch, S.P. (1991), *Mater. Sci. Eng.*, **A136**, 25 - 43.

McDarmaid, D.S. and Peel, C.J. (1989), in 'Aluminium - Lithium Alloys', *Proc. 5th Inter. Aluminium - Lithium Conf.*, **Vol.** II, ed. Sanders, T.H. and Starke, E.A., Mater. and Components Eng. Pub. Ltd., Brimingham, U.K., 993 - 1002.

Peel, C.J. and McDarmaid, D.S. (1989), *Aerospace.*, **16**, 18 - 23.

Starke, E.A. and Lin, F.S. (1982), *Metall. Trans. A.*, **13A**, 2259 - 2269.

Suresh, S. and Vasudevan, A.K. (1986), *Mater. Sci. Eng.*, **79**, 183 - 190.

Suresh, S., Vasudevan, A.K., Tosten, M. and Howell, P.R. (1987), *Acta Metall.*, **35,** 25 - 46.

Wanhill, R.J.H. (1994), *Fatigue,* **16**, 3 - 20.

Wanhill, R.J. H., Schra, L. and 't Hart, W.G.J. (1992), *ASTM STP 1157*, American Society for Testing and Materials, Philadelphia, USA, 224 - 240.